

Geophysical Research Letters[®]

RESEARCH LETTER

10.1029/2022GL099390

Key Points:

- Discovery of similarity between high frequency-induced stimulated Brillouin scattering (SBS) and incoherent scatter radar spectrum
- Intelligent stimulated electromagnetic emission inversion architecture proposed by incorporating physical insights within an artificial neural network approach
- Novel ionospheric electron temperature inversion based on SBS and downshifted maximum spectral lines

Correspondence to:

H. Y. Fu,
haiyang_fu@fudan.edu.cn

Citation:

Fu, H. Y., Jiang, M. L., Vierinen, J., Häggström, I., Rietveld, M. T., Varberg, E., et al. (2022). A stimulated emission diagnostic technique for electron temperature of the high power radio wave modified ionosphere. *Geophysical Research Letters*, 49, e2022GL099390. <https://doi.org/10.1029/2022GL099390>








Received 4 MAY 2022
Accepted 2 AUG 2022
Corrected 23 AUG 2022

This article was corrected on 23 AUG 2022. See the end of the full text for details.

Author Contributions:

Conceptualization: H. Y. Fu, Y. Q. Jin
Formal analysis: H. Y. Fu, M. L. Jiang, J. Vierinen, I. Häggström, M. T. Rietveld, E. Varberg, H. Sato
Supervision: J. Wu, Y. Q. Jin
Writing – original draft: H. Y. Fu
Writing – review & editing: M. T. Rietveld, W. A. Scales

A Stimulated Emission Diagnostic Technique for Electron Temperature of the High Power Radio Wave Modified Ionosphere

H. Y. Fu^{1,2} , M. L. Jiang², J. Vierinen³ , I. Häggström⁴, M. T. Rietveld^{3,5} , E. Varberg^{3,5} , H. Sato⁶ , J. Wu⁷, W. A. Scales⁸ , and Y. Q. Jin^{1,2} 

¹Key Laboratory for Information Science of Electromagnetic Waves (MoE), Fudan University, Shanghai, China, ²School of Information Science and Technology, Fudan University, Shanghai, China, ³UiT The Arctic University of Norway, Tromsø, Norway, ⁴EISCAT Scientific Association, Kiruna, Sweden, ⁵EISCAT Scientific Association, Tromsø, Norway, ⁶DLR Institute for Solar-Terrestrial Physics, Neustrelitz, Germany, ⁷China Research Institute of Radiowave Propagation, Qingdao, China, ⁸Bradley Department of Electrical and Computer Engineering, Virginia Polytechnic Institute and State University, Blacksburg, VA, USA

Abstract We report observations of stimulated electromagnetic emission (SEE) induced by high power high frequency (HF) radio waves near the third electron gyroharmonic ($3f_{ce}$) at European Incoherent Scatter Radar (EISCAT). It is discovered that stimulated Brillouin scattering (SBS) spectrum behaves similarly as spectral ion lines of the incoherent scatter radar (ISR) for HF pumping frequency above $3f_{ce}$. The SBS spectral width shows correlation with electron to ion temperature ratio T_e/T_i . A new inversion method is proposed by incorporating the SBS spectral width within an artificial neural network approach to achieve electron temperature inversion for ionospheric turbulent plasmas. This work provides a potential new technique to diagnose parameters in the modified ionosphere when the ISR is not available.

Plain Language Summary Nonlinear interaction of high-power electromagnetic waves and magnetized plasmas produces a plethora of fundamental phenomena. Stimulated electromagnetic emissions (SEEs) arises from nonlinear interaction and induces plasma turbulence observable by incoherent scatter radars (ISR). It is important to compare SEE and ISR spectral lines for understanding nonlinear physics in the resonance regime. The SEE-based methods may provide complimentary diagnostic tools to the traditional ISR theory. In addition, the SEE-based inversion theory and method is still lacking due to nonlinear wave-wave and wave-particle interaction. The physical correlation between SEEs and ISR spectra will provide benefit for better inversion techniques. This work reports experimental observation and parameter inversion of stimulated Brillouin scatter (SBS) at EISCAT (European Incoherent Scatter Radar). We successfully discover similarity between the ISR ion lines and SBS near the third electron gyroharmonic by high power radio waves at EISCAT. A new diagnostic technique based on SEEs have been developed using physical model and an artificial neural network approach. The inversion of SEEs overcomes the non-Maxwellian limitations on ISR measurements. These observations demonstrate a physical intrinsic correlation between ISR ion and SBS lines, which provides possibilities for developing new inversion techniques based on SBS in comparison with well-known ISR theory.

1. Introduction

Stimulated electromagnetic emissions (SEE) in the ionosphere arise from plasma turbulence induced by HF high-power electromagnetic waves due to parametric decay instabilities (PDI) (Leyser et al., 1989; Stubbe et al., 1984). The complexity of SEE arises from the wave-wave and wave-particle interaction mechanisms in magnetized plasmas, particularly for pumping near electron gyro-harmonics (Stubbe & Kopka, 1990). The first SEE experiments by HF pump in the ionosphere dates back to the 1980s by Thidé at EISCAT (Thidé et al., 1982). Afterward, SEE have been studied at other HF facilities at Sura, HAARP and Arecibo to understand the excitation mechanism and serve as diagnostics in combination with other remote sensing tools such as incoherent scatter radar (ISR) (Bernhardt et al., 2009, 2010; Eliasson et al., 2021; Fu et al., 2015, 2018; Leyser, 2001; Leyser et al., 1989; Mahmoudian, Nossa, et al., 2019; Mahmoudian, Senior, et al., 2019; Norin et al., 2009). SEE in space plasmas are physically complicated nonlinear processes and it is currently difficult to develop comprehensive physics-based models since the characteristic spectral lines are produced over a wide range of space and temporal scales. The investigation of the physical processes associated with SEE in space plasmas is crucial not only for

diagnostic purposes but also for understanding fundamental physics which may have linkages to those investigated in nonlinear optics (Kruer, 1988).

Since the 1960s, incoherent scatter radar (ISR) operating at ultrahigh frequency (UHF) have been used to measure weak thermal fluctuations (Thompson Scatter) in ionospheric plasmas (Dougherty & Farley, 1960; Evans, 1969) based on original incoherent scattering theory (Farley et al., 1961; Fejer, 1961). It is well known that analysis of the ISR ion line spectra to provide ionospheric plasma parameters, called the ISR inversion, is valid when assuming a Maxwellian electron velocity distribution (Evans, 1969). It is traditionally recognized that ISR and SEE spectra involves different physical processes and inversion methods for obtaining diagnostic information (Stubbe & Kopka, 1990). The electron temperature serves a crucial role for understanding the wave-particle and wave-wave interaction. However, this implies the important question: Is there strong correlation between ISR ion line and SEE spectra? If this is the case, can SEE become a viable alternative diagnostic for the strongly nonlinear turbulent plasma when ISR is inaccurate or unavailable? Previous SBS-based inversion methods (Bernhardt et al., 2009; Fu et al., 2020) for electron temperature relies on the linear dispersion relation without considering the SBS spectral width. Another drawback that cannot be ignored is that the SBS excitation threshold requires higher than other commonly observed SEE such as downshifted maximum (DM), which however have not been attempted for electron temperature inversion. Therefore, this work aims to develop the SEE-based method based on complex SEE features that may provide diagnostics tool when the ISR measurement is not available or not valid. This letter reports experimental discovery of upredicted similarity between SBS and ISR ion line spectra near the third electron gyroharmonic at EISCAT as well as novel SEE-based inversion methods. A new inversion method is proposed by incorporating the SBS spectral width within an artificial neural network approach to achieve electron temperature inversion. Also, we investigate the electron temperature inversion based on another stimulated downshifted maximum (DM) in combination with SBS for the first time. The data includes measurements of SEE and enhanced ion lines by the UHF incoherent scatter radar at EISCAT.

2. Experimental Setup

The experiment at EISCAT was conducted on 19 October 2020 with the HF transmitter operating at O-mode polarization with full power. The beam was transmitted in a quasi-continuous wave mode along the magnetic field. The HF pump frequency is stepped every 10 s from 4.0 to 4.46875 MHz in 3.125 kHz steps through the third electron gyroharmonic $3f_{ce}$. The 30-min cycle includes 25 min plus 10 s (1,510 s) for heating “on” and 290 s for heating “off.” Note this implies there are four 30-min cycles with pump turned on at 10:00, 10:30, 11:00, 11:30 between 10 and 12 UT depicted in Figure 1. For HF transmitter at pump frequency 4.28125 MHz, the Effective Radiated Power (ERP) is estimated to be 173.8 MW based on the beam pattern calculated using the numerical electromagnetic code developed by A. Senior with contributions by M. T. Rietveld, which is freely available at <https://gitlab.com/andrewsenior/heatererp>.

The SEE receiver was installed in Skibotn, a suburb of Tromsø, about 13 km north northwest (NNW) of the heater facility in Ramfjordmoen, separated by a mountain range. The antenna was a Well brook active loop antenna. The sampled SEE data are processed with the short-time Fourier Transform (STFT) to yield low frequency sideband spectra of the backscatter wave from the pump wave frequency.

The 931 MHz UHF radar was operated in the Beata mode, which enables measurement from 70 to 680 km with a minimum of 5 s time resolution and 3.5 km range resolution. The UHF radar data was integrated for 10 s with approximately 14 km resolution near the reflection region. The UHF incoherent scatter radar provides ionospheric measurement, including electron temperature T_e , electron density N_e , raw electron density N_r , electron and ion temperature ratio T_e/T_i , and plasma flow velocity V_d . A dynasonde co-located with EISCAT with a sounding every 2 min provides the bottomside electron density profile of the ionosphere.

3. Experimental Results and Analysis

Figure 1 shows the spectral comparison of (a) the SBS spectral line due to ion acoustic waves induced by HF heating and (b) the ion line for the UHF ISR radar. It is noted that the two independent spectra behave similar near $3f_{ce}$. Using the International Geomagnetic Reference (IGRF) model, the third electron gyroharmonic frequency is estimated to be $3f_{ce} \sim 4.21$ MHz. The first common characteristic is that as HF heating is turned on, the

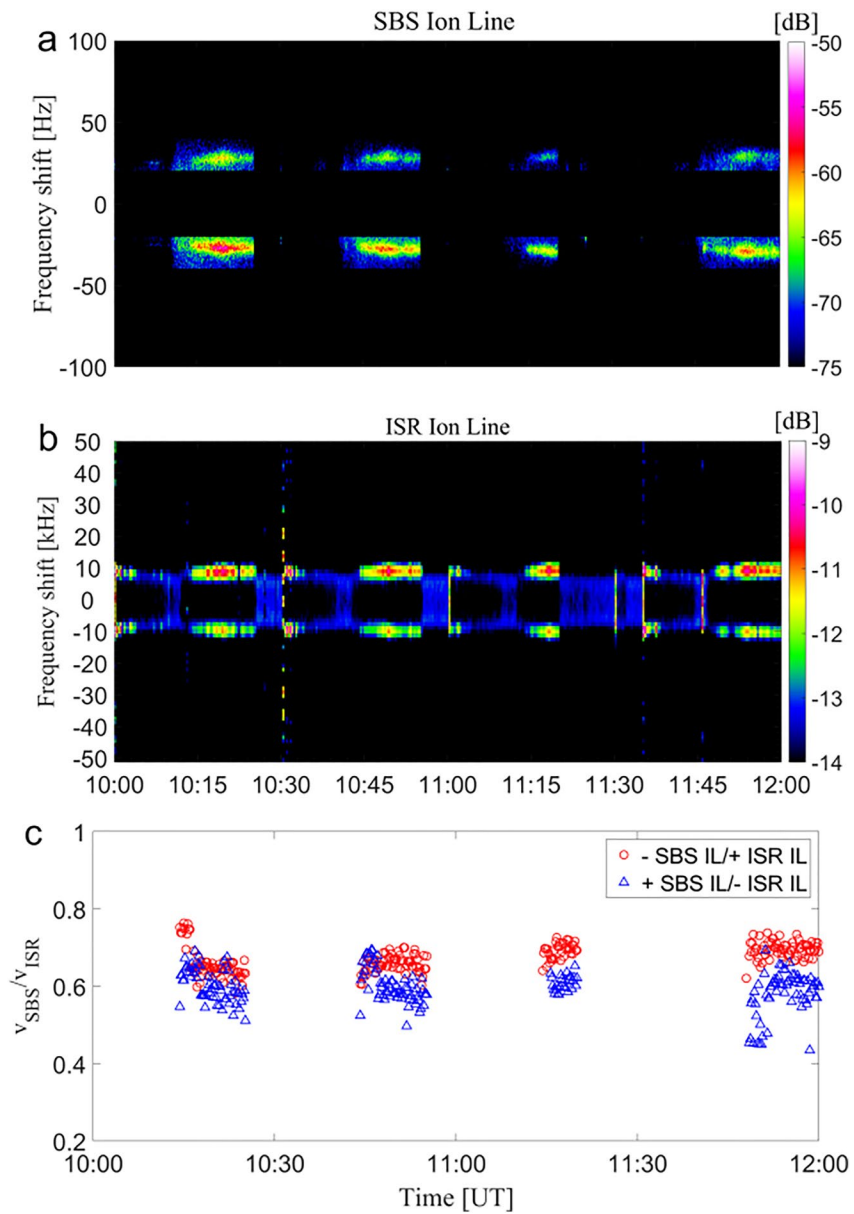


Figure 1. Comparison of ion line spectra for stimulated Brillouin scattering (SBS) and European Incoherent Scatter Radar ultrahigh frequency incoherent scatter radar (ISR) for high frequency pumping near $3f_{ce}$, including (a) SBS spectra by heating, (b) enhanced ISR ion line spectra, and (c) the Doppler velocity ratio of SBS and ISR ion line (IL) spectra. The SBS spectra is centered at $\pm(26\text{--}29)$ Hz and the ISR ion line spectra at ± 8.9 kHz. Cycle I, II, III, IV starts at 10:00, 10:30, 11:00, 11:30 using frequency stepping upwards scheme near $3f_{ce}$. It is noted that the spectral intensities and widths of the ISR and SBS ion lines increase substantially for $f_{HF} > 3f_{ce}$.

spectral intensities and widths of the ISR and SBS ion lines increase substantially for $f_{HF} > 3f_{ce}$. Another common characteristic is that both upshifted and downshifted spectral lines exhibit an asymmetry in power intensity. The frequency offset of the ISR ion acoustic lines $f_{\pm ION}$ is centered at ± 8.9 kHz with bandwidth ~ 4.7 kHz, whereas the SBS ion acoustic line $f_{\pm SBS}$ is approximately at ± 28 Hz with linewidth ~ 8 Hz. The behavior of both ion lines on the pump wave frequency and the opposite asymmetry prompted us to examine the correlation between SBS and ISR in detail.

To analyze correlation between SBS and ISR, we calculate the Doppler frequency f_d roughly estimated as $f_d = 2V_r/\lambda \approx 2f_0V_r/c$, where V_r is the ion-acoustic velocity along the line of sight and c is the speed of light. Here, λ is the wavelength at f_0 for either HF pump frequency f_{HF} or the ISR frequency f_{UHF} . The upshifted/downshifted

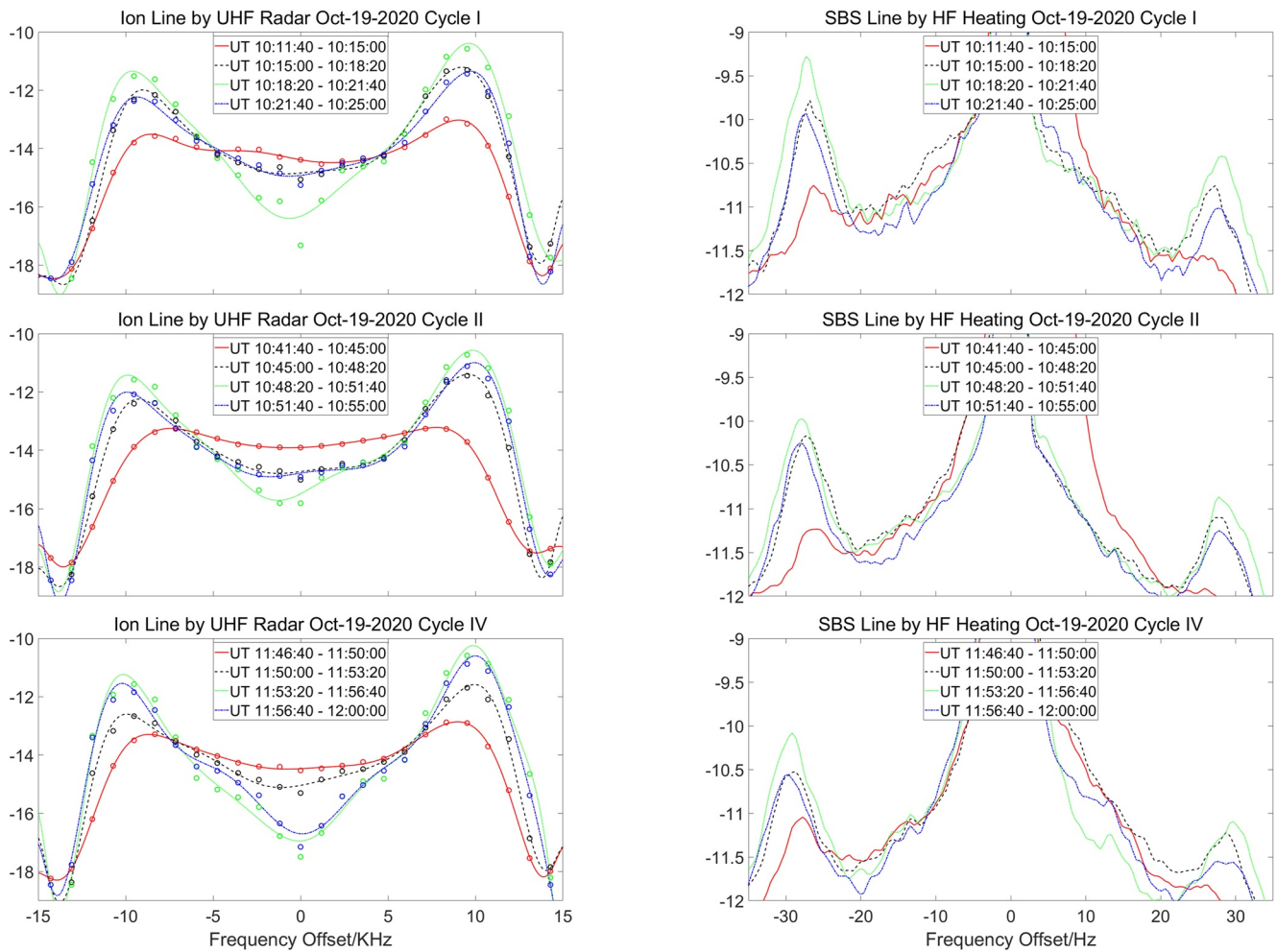


Figure 2. Comparison of one-dimensional averaged incoherent scatter radar (ISR) and stimulated Brillouin scattering (SBS) ion line spectra reveals similarity near $3f_{ce}$. The top, middle, bottom panel shows relative power intensity of the 1-D averaged ISR (left) and SBS (right) ion line spectra within time interval 200 s between 4.21875 and 4.46875 MHz for Cycle I (10:11:40–10:25:00 UT), Cycle II (10:41:40–10:55:00 UT), and Cycle IV (10:46:40–12:00:00 UT), respectively.

SBS frequency offset $f_{\pm\text{SBS}}$ in Figure 1a and the ISR ion line frequency offset $f_{\pm\text{ION}}$ in Figure 1b are calculated based on the maximum spectral power density, respectively. The ratio $\alpha = (f_{\text{SBS}}/f_{\text{HF}}) : (f_{\text{ION}}/f_{\text{UHF}})$ is compared in Figure 1c, where f_{SBS} is the SBS ion line by $f_0 = f_{\text{HF}}$ and f_{ION} is the ISR ion line by $f_0 = f_{\text{UHF}}$. The ratio of velocity from SBS and ISR ion lines can be expressed as $\alpha = V_{\text{SBS}}/V_{\text{ION}}$ as in Figure 1c. The Doppler velocity ratio α between 0.6 and 0.7 may indicate that the SBS and ISR ion line satisfy the Doppler frequency as $f_d \propto 2f_0V_r$, which corresponds to similar ion acoustic waves with ion acoustic speed. Such discrepancy from $\alpha \sim 1$ may be explained based on the ISR and SBS scattering mechanism. The ISR lines correspond to the ion-acoustic wave at approximately half the ISR vacuum wavelength, while for the SBS lines, the EM wave is near its cut-off frequency, corresponding to an ion acoustic wavelength longer than half the vacuum wavelength (Eliasson et al., 2021).

The comparison of one-dimensional (1-D) averaged spectra for ISR and SBS ion line is depicted in Figure 2. The ion line spectrum for ISR and SBS grows similarly near $3f_{ce}$ for 4.21875 MHz (red line) and then saturates for 4.34375–4.40625 MHz (green line) for Cycle I (10:11:40–10:21:00 UT), Cycle II (10:41:40–10:55:00 UT) and Cycle IV (10:46:40–12:00:00 UT), respectively. It is noted that downshifted (Stokes) SBS shows enhanced power relative to upshifted (anti-Stokes) SBS, which on the contrary, shows opposite asymmetry compared to the ISR ion lines. The downshifted (Stokes) SBS shows stronger power than the upshifted (anti-stokes) spectra due to the SBS instability as explained in Bernhardt et al. (2009). The enhanced positive Doppler of the ISR ion line in Figure 2 correspond to ion drift velocity downwards to the ISR radar for raw electron density as will be shown in Figure 3b. It is noted that the valley of the ISR spectrum is different from the SBS which instead has

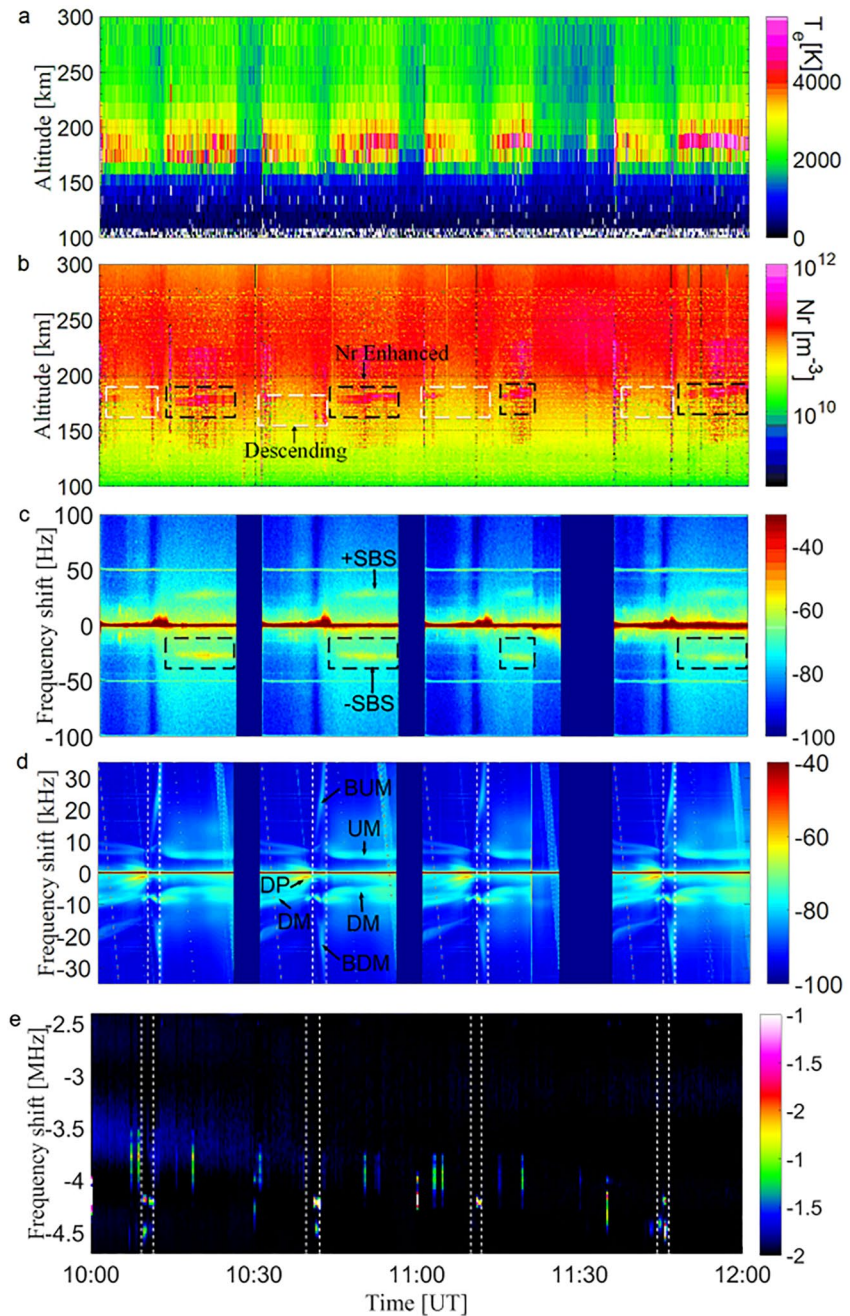


Figure 3. Simultaneous measurement of stimulated electromagnetic emissions by high frequency pumping and plasma parameters by the ultrahigh frequency incoherent scatter radar near the third electron gyro-harmonic $3f_{ce}$ at European Incoherent Scatter Radar on 19 October 2020. Each panel shows (a) electron temperature T_e from incoherent scatter radar (ISR), (b) raw electron density N_r from ISR, (c) narrowband stimulated electromagnetic emission (SEE) spectrogram power within 100 Hz showing stimulated Brillouin scattering (SBS), (d) wideband SEE spectrogram within 50 kHz, including downshifted/upshifted maximum (DM, UM), broad upshifted/downshifted maximum (BUM, BDM) within vertical white dashed lines, downshifted peak, and (e) the ISR plasma line showing enhanced power intensity within vertical white dashed lines near $3f_{ce}$.

a sharp maximum in the center due to the reflected HF pump wave. Although the SBS and ISR ion lines are not completely identical, these spectral observations in Figures 1 and 2 demonstrates similarity and correlation between the ISR ion and SBS lines. This may provide possibilities for developing new inversion techniques based on SBS in comparison with well-known ISR theory.

Figure 3 shows simultaneous measurement of (a) electron temperature T_e , (b) raw electron density N_r by ISR, (c) narrowband SEE, and (d) wideband SEE spectrum. The ISR time resolution is 10 s in Figures 3a and 3b and 20 s for SEE in Figures 3c and 3d. According to Figure 3a, the heated altitudes occur between 174 and 200 km according to T_e measured by the ISR ion line. Raw electron density may not refer to real electron density but corresponds to real increased back-scattering measurement with fine range resolution. The reflection height is estimated to be 187 km when pumping frequency f_0 matches the plasma frequency f_p . It is noted that the upper-hybrid resonance f_{uh} occurs several kilometers below plasma resonance reflection f_p , while the ISR cannot resolve this range resolution. We take the measured value of the height 186–189 km as the reference parameter for subsequent cycles.

There exists asymmetry of enhanced electron temperature T_e , raw electron density N_r and SBS for pumping above $3f_{ce}$ compared to below in Figures 3a–3c. These upshifted and downshifted SBS emissions in Figure 3c within 100 Hz appear at approximately -27 Hz, that approximately occurs at 14 min ($f_{HF} = 4.2594$ MHz) after heating on at 10:00, 10:30, 11:00, 11:30 for each cycle, respectively. It is noted that SBS appears only after $f_{HF} > 3f_{ce}$, which may be due to pump power below threshold for $f_{HF} < 3f_{ce}$. Figure 3d shows wideband SEE spectrogram due to different parametric decay processes in magnetized plasmas, such as downshifted maximum (DM) associated with the lower hybrid wave, and others including downshifted peak (DP) and broad upshifted maximum (BUM). It is noted that the BUM in Figure 3d corresponds to enhanced plasma lines in Figure 3e within dashed interval in frequency range of 4.175–4.228 MHz near $3f_{ce}$. The descending layer in the white dashed box in Figure 3b starts from the resonance height when the heater turns on and then descends downwards producing discrete enhanced N_r which is in consistent with observations of the BUM in Figure 3d and plasma lines in Figure 3e within the dashed white lines. The descending raw electron density near $3f_{ce}$ in Figure 3b shows similar descending raw electron density for $4f_{ce}$ (Mahmoudian, Nossa, et al., 2019; Mahmoudian, Senior, et al., 2019) at EISCAT.

Now, we focus on electron temperature inversion based on SBS observation induced by HF pumping as described above. Because of the dependence of the SBS spectral line offset from f_{HF} on ion acoustic waves, we calculate electron temperature using SBS only. The wave matching condition for stimulated Brillouin scattering in magnetized ionospheric plasmas (Bernhardt et al., 2009; Norin et al., 2009) are $\omega_0 = \omega_s + \omega_L$ and $\mathbf{k}_0 = \mathbf{k}_s + \mathbf{k}_L$, where ω is the wave frequency, \mathbf{k} is the wave propagation vector, and the subscript 0, s, and L denotes the pump, scattered, and low-frequency waves, respectively. Based on the wave matching condition, the ion acoustic speed at the upper hybrid UH matching altitude for $\omega_0 = \omega_{uh}$ for the O-mode in Bernhardt et al. (2009) is

$$c_{IA} = \frac{c\omega_{IA}}{2\sqrt{\Omega_e\omega_0}} \sqrt{\frac{\Omega_i^2 - \omega_0^2}{\Omega_i^2 \cos^2 \theta - \omega_0^2}} \sqrt{\frac{\omega_0 + \Omega_e \cos \theta}{\omega_0 \cos \theta + \Omega_e}} \quad (1)$$

where ω_0 is the pump wave angular frequency, ω_{IA} is the ion acoustic wave angular frequency, Ω_i is the ion cyclotron angular frequency, Ω_e is the electron cyclotron angular frequency and c is the speed of light, respectively. Here, θ is the angle between the ion acoustic wave vector \mathbf{k} and the geomagnetic field \mathbf{B} . The wave angle θ is estimated to be $\sim 8^\circ$ based on ray tracing calculation (Fu et al., 2013) at the upper hybrid UH resonance altitude. The ion acoustic wave speed depends on the electron temperature T_e and ion temperature T_i as

$$c_{IA} = \sqrt{\frac{T_e + 3T_i}{m_i}} \quad (2)$$

According to the ISR theory (Evans, 1969), T_e/T_i is determined by the ion line peak-to-valley ratio, which may be used for inversion based on the SBS spectrum. This correlation between ISR and SBS ion line frequency shift and opposite asymmetry provides physical evidence for new inversion techniques. Compared to the existing ISR theory, we lack theory to directly construct the relationship between the SBS spectrum and ionospheric parameters.

Although enhanced T_e by ISR fluctuates for heating above $3f_{ce}$ in Figure 4a, an important phenomenon is that the SBS linewidth is correlated with T_e/T_i measured by ISR. Figure 4a compares the SBS linewidth with T_e/T_i measured by ISR. It is observed that the downshifted SBS linewidth is correlated with the measured T_e/T_i . For the linewidth extraction of SBS with power reduced to a certain low negligible level threshold, we let the time domain signal pass through a low-pass filter and then we downsample the time domain signal. After downsampling, the short-time Fourier transform is used to transform the data to the frequency domain with wavelet filtering. Based on the extraction method as described above, the derived linewidth from SBS spectrum is smooth. Therefore,

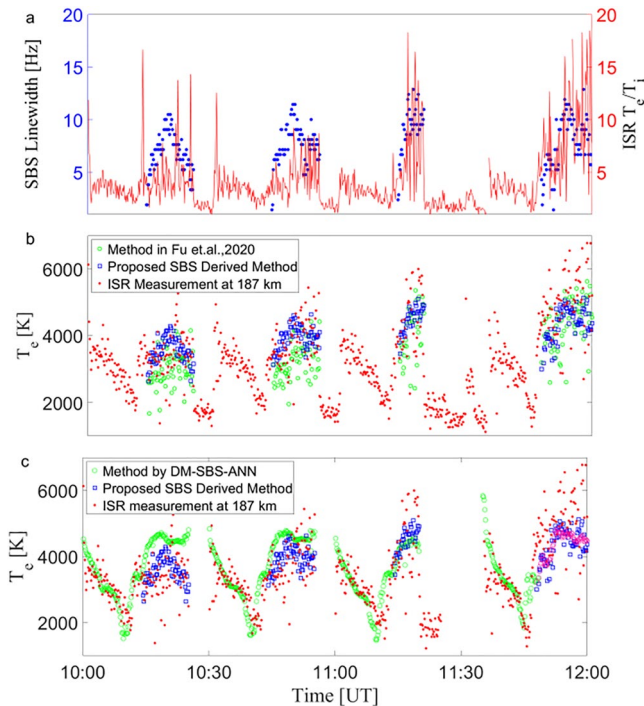


Figure 4. Comparison of extracted stimulated Brillouin scattering (SBS) linewidth (blue dot) and T_e/T_i (red line) measured by incoherent scatter radar (ISR) (a) for inversion. The T_e by the proposed SBS method (blue square) is compared with the ISR measurement and previous work in Fu et al. (2020) in panel (b). The DM-ANN inversion with SBS labeling is accomplished in panel (c) to retrieve T_e without SBS. The pink circle denotes training data and green for test data for artificial neural network.

we incorporate the SBS linewidth to substitute T_e/T_i in combination with Equations 1 and 2 to calculate T_e , namely called “the proposed SBS derived method.” We only use the downshifted SBS sideband in this work.

Figure 4b shows the results of electron temperature based on the proposed SBS derived method on 19 October 2020. We compare T_e by the proposed SBS method (blue square) in Figure 4b with previous work (green circle) (Fu et al., 2020) and the ISR measurement at 187 km. When there exists SBS mostly for above $3f_{ce}$, it is noted that T_e by the SBS method is 594–969 K lower than the ISR measurement. The averaged discrepancy between the SBS method and the ISR measurement is approximately 16%–22%. The standard deviation of T_e by the SBS derived method is 384–494 K less than 692–954 K by ISR. The inversion based on the SBS method is smooth, that may be important for labeling for artificial neural network (ANN).

Since the threshold of SBS is difficult to excite for the entire heating period, particularly below $3f_{ce}$, we investigate another commonly observed SEE spectral line, namely the downshifted maximum (DM). Previous studies have suggested that there exists a correlation between the DM spectral line and electron temperature enhancement (Fu et al., 2020). To our knowledge, there is no simple theory to describe direct correlation between DM spectral lines and electron temperature, and thus we attempt to characterize the unknown relationship by ANN.

Figure 4c shows the results of electron temperature by the DM-SBS-ANN inversion method. The DM-SBS-ANN inversion method uses neural network techniques to yield the electron temperature from the DM and SBS spectra. A brief description of the DM-SBS-ANN is given as following. First of all, the labeled T_e are derived from the SBS spectrum in the training data. For training, only data for pumping above $3f_{ce}$ between 11:35 and 12:00 UT in Cycle 4 are adopted. The labels T_e/T_i are obtained from the SBS linewidth method as described above. The DM spectra at each time is used as the input to the neural network. The remaining data in Cycles I, II, III are adopted for the test set. We simply adopted a deep feed-forward networks for validation. This neural network consists of the input layer, three hidden layers and the output layer (Zhang et al., 2020). Each hidden layer has 256, 512, and 512 neurons with ReLU activation function, respectively. In order to solve uneven distribution of the training set, we perform unsupervised training on a portion of the Cycle II and Cycle IV data for $f_0 < 3f_{ce}$, and the loss function is designed based on the temporal gradient over that portion of time. This method can be also used for predicting T_e/T_i .

Finally, the inversion error based on the SBS-derived method and DM-SBS-ANN methods are compared. The SBS-based method can predict electron temperature once SBS is excited mostly for above $3f_{ce}$ when enhanced electron temperature by ISR measurement produces relative large fluctuations due to non-Maxwellian distribution. It is difficult to define true electron temperature for heating above $3f_{ce}$ with strongly disturbed plasma. Since SBS requires higher threshold than DM, the DM-ANN algorithm achieves inversion for the entire heating cycle. For pumping below $3f_{ce}$ without SBS, electron temperature by the ISR measurement is reasonable as a benchmark, the absolute discrepancy of the DM-ANN algorithm is less than 500 K. For pumping above $3f_{ce}$ with SBS, the absolute discrepancy of the DM-ANN algorithm is up to 1000 K in comparison with the ISR measurement. The DM-ANN algorithm with SBS labeling shows better agreement with ISR than that by the SBS-derived method.

The correlation between electron density and SEE is another important question for understanding the HF induced effects and potential electron density diagnostics. Figure 5 shows (a) the heating geometry; (b) the ISR raw electron density enhancement associated with SBS; (c) simultaneous observation of GLONASS navigation signals received at two sites, one at the heating facility at EISCAT and one at Tromsø (14 km apart), and (d) ISR raw electron density and plasma lines, respectively. Ionospheric density perturbation in the GLONASS signal is

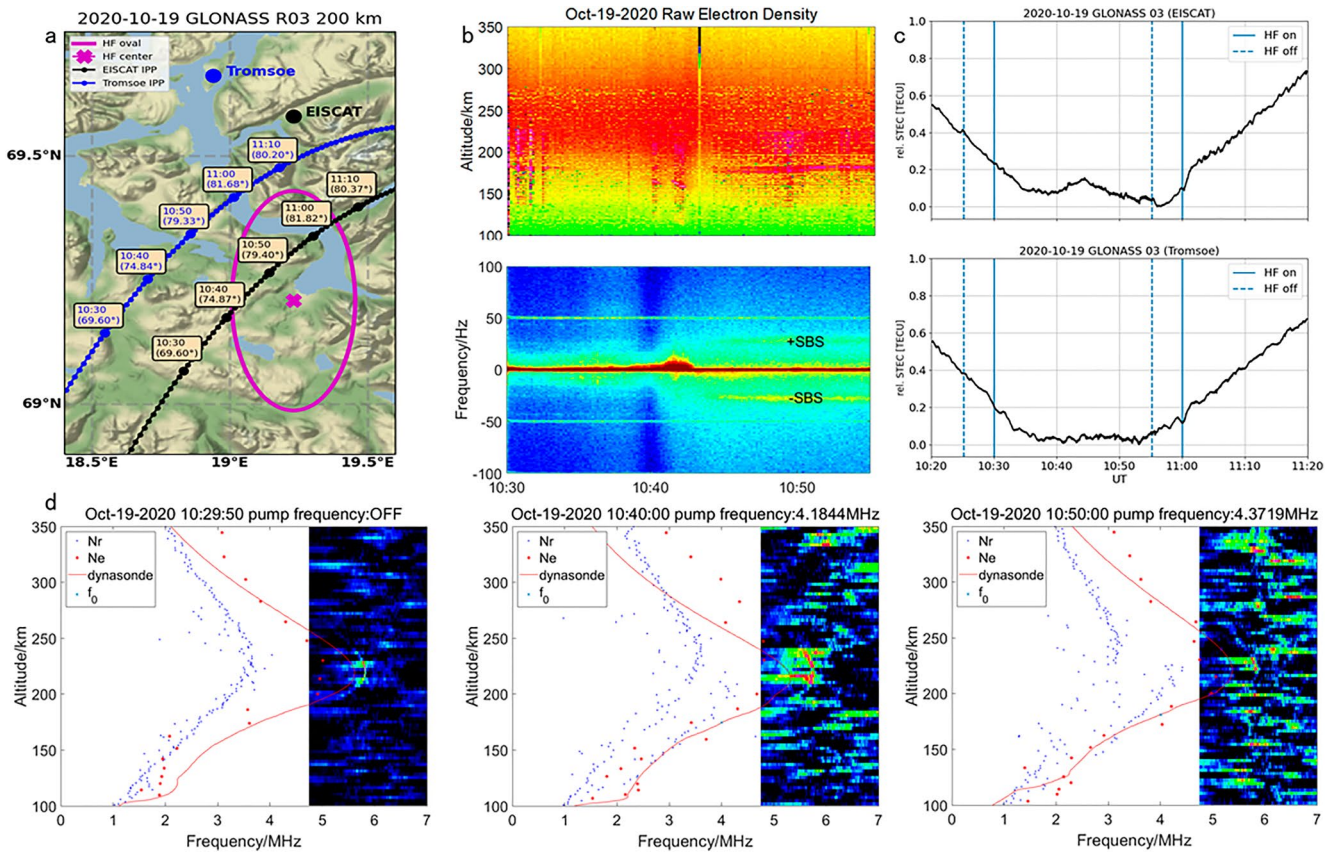


Figure 5. Simultaneous measurement of stimulated Brillouin scattering (SBS) and disturbed electron density with disturbed GLONASS signals in Cycle II during 10:00–10:30 UT for pumping near the third electron gyro-harmonic $3f_{ce}$ at European Incoherent Scatter Radar (EISCAT) on 19 October 2020. (a) GLONASS satellites flying geometry over the EISCAT region, showing the locations of ionospheric piercing point (IPP) at altitude 200 km. The purple ellipse shows the high frequency impact oval for the beamwidth of 7° . (b) Raw electron density N_r by ISR (up) and SBS spectrogram power intensity (down), (c) Slant TEC observation by 50 Hz GNSS receivers at EISCAT and Tromsø, (d) Electron density N_e by ISR (red line) and Dynasonde (red dots) in comparison with raw electron density N_r (blue dots) for pumping off (at 10:29:50 UT), below $3f_{ce}$ (4.1844 MHz at 10:40:00 UT) and above $3f_{ce}$ (4.3719 MHz at 10:50:00 UT), where the dark area on right refers to the ISR plasma line with power intensity encoded in color.

measured in Total Electron Content (TEC) which is integrated electron density between the satellite and receiver. The raw electron density enhancement at time 10:30–11 in Cycle II in Figure 5c corresponds to deviation of relative TEC from the background density starting from 10:38 UT observed at EISCAT receiver. The peak perturbation is approximately 0.1 TECU ($1\text{TECU} = 10^{16}$ electrons/m²) at 10:44 UT. The TEC perturbation is observed to be continued while the satellite signal intersected the estimated HF impact area until the HF off at 10:55:10 UT. Such TEC perturbation is not clearly observed at Tromsø receiver where the ionospheric volume intersected by the satellite signal has larger distance from the HF beam center. This observation shows evidence that the plasma density perturbation associated with SBS may result in the enhancement of electron density near the HF beam center and lead to navigation satellite signal perturbation. The correlation may indicate potential electron density inversion based on navigation signals as well as SBS and ISR radars.

Based on “raw electron density” N_r profile on the bottom panel of Figure 5, the electron density is disturbed from the foF2 height at 210 km down to 150 km. The raw electron density enhancement is closely correlated with SBS in Figure 5b as also observed in Figure 3. The electron density fluctuation not only occurs at the resonance region, that may arise from propagation of SBS ion acoustic waves (Eliasson et al., 2021). The enhanced “raw density” may not mean enhanced electron density but may be increased back-scattering from other processes like instabilities. The fact that N_r is much less than N_e is due to electron to ion temperature ratio T_e/T_i greater than 1 (Pinedo et al., 2014).

4. Conclusions

In conclusion, the EISCAT ionospheric modification experiment show similar ISR ion and SBS spectral line evolution for a pumping frequency above $3f_{ce}$. The discovery noted in this manuscript is that strong evidence has been presented relating the ISR ion line and SBS emissions which will facilitate and validate development of robust SBS-based diagnostics. The physical correlation between SBS and ISR ion lines indicate that inversion based on SEE may potentially overcome the ISR non-Maxwellian limitation for strongly disturbed plasma turbulence during HF heating. The newly developed inversion technique using the SBS spectral width and the DM-SBS-ANN approach for electron temperature measurement may become an alternative for ISR if it is inaccurate or unavailable. Future work will consider advanced neural network to include temporal evolution for more robust ionospheric parameter inversion (Zhang et al., 2022).

Data Availability Statement

The ISR radar data are available from <https://portal.eiscat.se/rtg/gup.cgi?U>. The SEEs data are available from <https://doi.org/10.5281/zenodo.6960914>.

Acknowledgments

EISCAT is an international association supported by research organizations in China (CRIRP), Finland (SA), Japan (NIPR and ISEE), Norway (NFR), Sweden (VR), and the United Kingdom (UKRI). The authors from Fudan University are also supported by China National Science Foundation (42074189) and Shanghai Science and Technology Committee with Grant 19ZR1403900.

References

- Bernhardt, P. A., Selcher, C. A., Lehmberg, R. H., Rodriguez, S., Thomason, J., McCarrick, M. J., & Frazer, G. J. (2009). Determination of the electron temperature in the modified ionosphere over HAARP using the HF pumped Stimulated Brillouin Scatter (SBS) emission lines. *Annales Geophysicae*, 27(12), 4409–4427. <https://doi.org/10.5194/angeo-27-4409-2009>
- Bernhardt, P. A., Selcher, C. A., Lehmberg, R. H., Rodriguez, S. P., Thomason, J. F., Groves, K. M., et al. (2010). Stimulated Brillouin scatter in a magnetized ionospheric plasma. *Physical Review Letters*, 104(16), 165004. <https://doi.org/10.1103/physrevlett.104.165004>
- Dougherty, J. P., & Farley, D. T. (1960). A theory of incoherent scattering of radio waves by a plasma. *Proceedings of the Royal Society of London. Series A. Mathematical and Physical Sciences*, 259, 79–99.
- Eliasson, B., Senior, A., Rietveld, M., Phelps, A. D. R., Cairns, R. A., Ronald, K., et al. (2021). Controlled beat-wave Brillouin scattering in the ionosphere. *Nature Communications*, 12(1), 6209. <https://doi.org/10.1038/s41467-021-26305-9>
- Evans, J. V. (1969). Theory and practice of ionosphere study by Thomson scatter radar. *Proceedings of the IEEE*, 57(4), 496–530. <https://doi.org/10.1109/proc.1969.7005>
- Farley, D. T., Dougherty, J. P., & Barron, D. W. (1961). A theory of incoherent scattering of radio waves by a plasma II. Scattering in a magnetic field. *Proceedings of the Royal Society of London. Series A. Mathematical and Physical Sciences*, 263, 238–258.
- Fejer, J. A. (1961). Scattering of radio waves by an ionized gas in thermal equilibrium in the presence of a uniform magnetic field. *Canadian Journal of Physics*, 39(5), 716–740. <https://doi.org/10.1139/p61-081>
- Fu, H. Y., Jiang, M. L., Wang, K. N., Wu, J., Li, Q. L., Rietveld, M. T., et al. (2020). Electron temperature inversion by stimulated Brillouin scattering during electron gyroharmonic heating at EISCAT. *Geophysical Research Letters*, 47(17), e2020GL089747. <https://doi.org/10.1029/2020gl089747>
- Fu, H. Y., Scales, W. A., Bernhardt, P. A., Briczinski, S. J., Kosch, M. J., Senior, A., Rietveld, M. T., et al. (2015). Stimulated Brillouin scattering during electron gyro-harmonic heating at EISCAT. *Annales Geophysicae*, 33(8), 983–990. <https://doi.org/10.5194/angeo-33-983-2015>
- Fu, H. Y., Scales, W. A., Bernhardt, P. A., Jin, Y. Q., & Briczinski, S. J. (2018). Asymmetry in stimulated emission polarization and irregularity evolution during ionospheric electron gyroharmonic heating. *Geophysical Research Letters*, 45(18), 9363–9371. <https://doi.org/10.1029/2018gl078957>
- Fu, H. Y., Scales, W. A., Bernhardt, P. A., Samimi, A., Mahmoudian, A., Briczinski, S. J., & McCarrick, M. J. (2013). Stimulated Brillouin scatter and stimulated ion Bernstein scatter during electron gyroharmonic heating experiments. *Radio Science*, 48(5), 607–616. <https://doi.org/10.1002/2013rs005262>
- Kruer, W. L. (1988). *The physics of laser plasma interactions*. Addison-Wesley.
- Leyser, T. B. (2001). Stimulated electromagnetic emissions by high-frequency electromagnetic pumping of the ionospheric plasma. *Space Science Reviews*, 98(3/4), 223–328. <https://doi.org/10.1023/a:1013875603938>
- Leyser, T. B., Thidé, B., Derblom, H., Hedberg, A., Lundborg, B., Stubbe, P., & Rietveld, M. T. (1989). Stimulated electromagnetic emission near electron cyclotron harmonics in the ionosphere. *Physical Review Letters*, 63(11), 1145–1147. <https://doi.org/10.1103/physrevlett.63.1145>
- Mahmoudian, A., Nossa, E., Isham, B., Bernhardt, P. A., Briczinski, S. J., & Sulzer, M. (2019). NSEE yielding electron temperature measurements at the Arecibo Observatory. *Journal of Geophysical Research: Space Physics*, 124(5), 3699–3708. <https://doi.org/10.1029/2019ja026594>
- Mahmoudian, A., Senior, A., Kosch, M., Scales, W. A., Rietveld, M. T., Isham, B., et al. (2019). Investigation of incoherent scatter radar spectra features with stimulated electromagnetic emissions at EISCAT. *Advances in Space Research*, 64(1), 159–170. <https://doi.org/10.1016/j.asr.2019.03.028>
- Norin, L., Leyser, T. B., Nordblad, E., Thidé, B., & McCarrick, M. (2009). Unprecedentedly strong and narrow electromagnetic emissions stimulated by high-frequency radio waves in the ionosphere. *Physical Review Letters*, 102(6), 065003. <https://doi.org/10.1103/PhysRevLett.102.065003>
- Pinedo, H., La Hoz, C., Havnes, O., & Rietveld, M. (2014). Electron-ion temperature ratio estimations in the summer polar mesosphere when subject to HF radio wave heating. *Journal of Atmospheric and Solar-Terrestrial Physics*, 118, 106–112. <https://doi.org/10.1016/j.jastp.2013.12.016>
- Senior, A. EISCAT HF facility radiated power model. Retrieved from <https://www.andrewsenior.org.uk/heatererp>
- Stubbe, P., & Kopka, H. (1990). Stimulated electromagnetic emission in a magnetized plasma: A new symmetric spectral feature. *Physical Review Letters*, 65(2), 183–186. <https://doi.org/10.1103/physrevlett.65.183>
- Stubbe, P., Kopka, H., Thidé, B., & Derblom, H. (1984). Stimulated electromagnetic emission: A new technique to study the parametric decay instability in the ionosphere. *Journal of Geophysical Research*, 89(A9), 7523–7536. <https://doi.org/10.1029/ja089ia09p07523>

- Thidé, B., Kopka, H., & Stubbe, P. (1982). Observations of stimulated scattering of a strong high-frequency radio wave in the ionosphere. *Physical Review Letters*, *49*(21), 1561–1564. <https://doi.org/10.1103/physrevlett.49.1561>
- Zhang, Y. Y., Fu, H. Y., Qin, Y. L., Wang, K. N., & Ma, J. (2022). Physics-informed deep neural network for inhomogeneous magnetized plasma parameter inversion. *IEEE Antennas and Wireless Propagation Letters*, *21*(4), 828–832. <https://doi.org/10.1109/lawp.2022.3149889>
- Zhang, Y. Y., Fu, H. Y., & Sui, Y. (2020). Neural network model for parameter inversion in electromagnetic wave and plasma interaction systems. *IEEE Transactions on Plasma Science*, *48*(6), 2143–2152. <https://doi.org/10.1109/tps.2020.2990459>

Erratum

In the originally published version of this article, the Author Contributions were incomplete, due to a proofreading error. The Author Contributions have since been corrected, and the present version may be considered the authoritative version of record.